


# STELLA+: Expanding the Research Potential for Long-Term Deep Brain Stimulation Studies in Freely-Moving Rodents

Franz Plocksties<sup>1</sup> <sup>a</sup>, Christoph Niemann<sup>1</sup>, Mareike Fauser<sup>2</sup>, Alexander Storch<sup>2</sup>, Dirk Timmermann<sup>1</sup> and Christian Haubelt<sup>1</sup>

<sup>1</sup>*Institute of Applied Microelectronics and Computer Engineering, University of Rostock, Germany*

<sup>2</sup>*Department of Neurology, University of Rostock, Rostock, Germany*


**Keywords:** Deep Brain Stimulation, Long-Term, Preclinical DBS Device, Adaptive DBS.

**Abstract:** Rodent models are essential for our understanding of Deep Brain Stimulation (DBS) mechanisms. However, most existing preclinical devices lack to support the broad experimental range required for modern DBS approaches. This paper presents the neurostimulation system STELLA+, which aims to enhance the scope of long-term DBS research in rodent models. STELLA+ upgrades the previous STELLA system that has been successfully used in several rodent studies. It features technical and architectural enhancements to increase performance and functionality for long-term DBS experiments. Initial *in vitro* findings demonstrate that STELLA+ delivers charge-balanced, current-controlled pulses with high accuracy across a range of stimulation settings up to a compliance voltage of 4.3 V. With a maximum current consumption of 25.1  $\mu$ A at 4.3 V in bilateral DBS-on mode, STELLA+ enables long-term experiments of 6.8 weeks using a 29 mAh lithium-ion battery. Additionally, STELLA+ includes a Bluetooth Low Energy module and the capability to acquire and compute on-board physiological data, enabling adaptive DBS applications. All these features are housed within a compact size of 21x14.5x4 mm, minimizing the impact on rodents. Compared to the other state-of-the-art DBS devices, STELLA+ demonstrates enhanced efficiency in stimulus generation and a uniquely comprehensive feature set.

## 1 INTRODUCTION

Deep Brain Stimulation (DBS) has emerged as a remarkable therapeutic approach for the management of various neurological and psychiatric disorders. By delivering electrical pulses to specific brain regions through implanted electrodes, DBS has shown significant results in symptom control and improving patients' quality of life. While the therapy is well-established for the treatment of movement disorders, such as Parkinson's disease, dystonia and tremor, its potential for other diseases is also being explored (Harmsen et al., 2020). However, the precise mechanisms by which DBS develops its therapeutic effects are still under active investigation (Hamani and Nóbrega, 2010; Jakobs et al., 2019). To address the open questions, preclinical *in vivo* experiments are essential. Rodent models have been widely employed in DBS research, allowing for investigations into electrophysiological, neurochemical and behavioral as-

pects (Ruiz et al., 2022). However, the progress of past studies has been impeded by runtime-restricted and bulky stimulation devices mounted on the rodent's head (Kölbl et al., 2016; Fluri et al., 2017; Pinnell et al., 2015; Pinnell et al., 2018; Forni et al., 2012; Liu et al., 2017; Ewing et al., 2013) or back (Kouzani et al., 2017; Badstuebner et al., 2017; Heo et al., 2015). These setups not only led to a significant strain on the animals, but also resulted in frequent device failures, e.g. due to cable breaks and mounting issues caused by the animals' movement. To overcome these limitations, the fully implantable stimulation device called STELLA (software defined implantable modular platform) was introduced, enabling reliable and long-term stimulation in rodents (Plocksties et al., 2021a). Furthermore, this device is highly suitable for sensitive behavioral studies in DBS research as it supports the refinement aspect of the 3R principles through the reduction of strain for the animals (Díez-Solinska et al., 2022). However, despite promising results from rodent studies conducted with STELLA (Plocksties et al., 2021a;

<sup>a</sup>  <https://orcid.org/0000-0003-0433-7703>

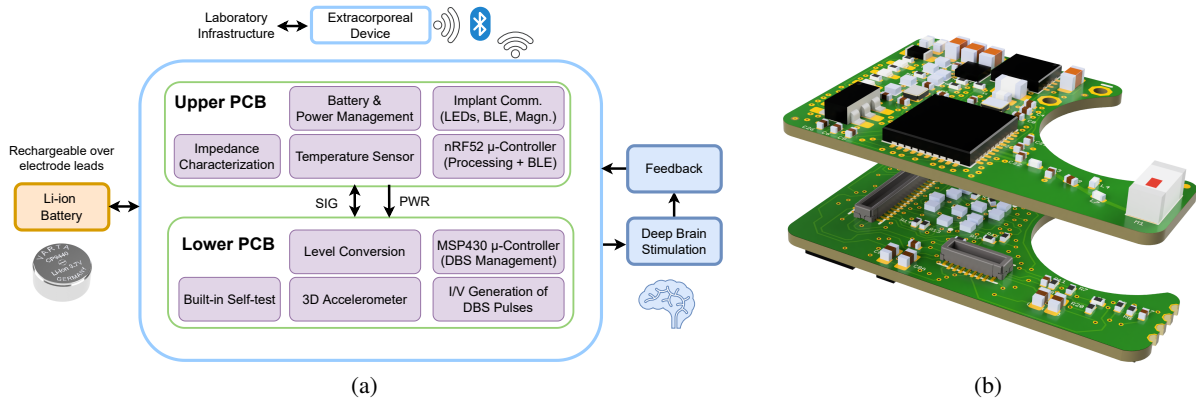


Figure 1: (a) STELLA+ system overview. (b) 3D design of the upper and lower PCB.

Plocksties et al., 2022; Koschay et al., 2022; Statz et al., 2023a; Statz et al., 2023b), a crucial gap remains. Like most other state-of-the-art preclinical DBS devices, STELLA has limitations in supporting a wide range of experimental applications, including research on adaptive DBS (aDBS). In clinical application, aDBS aims to optimize and individualize therapeutic outcomes by dynamically adjusting the stimulation parameters based on feedback data (Neumann et al., 2023). As research into suitable biomarkers and control methods is still ongoing, the translation of aDBS between clinical and laboratory settings is essential. To address this gap, a novel DBS device named STELLA+ has been designed that builds on the strengths of its predecessor while providing innovative features, which significantly increase experimental versatility. Key improvements include a more functional stimulation unit, multiple sensors, on-board signal processing capabilities and wireless connectivity, enabling researchers to explore diverse stimulation strategies in rodents.

This paper demonstrates the start-up phase of STELLA+, focusing on the technical implementation and performance analysis of the stimulation unit. Section 2 describes the technical specifications of STELLA+ in detail. Section 3 presents performance metrics of STELLA+ from *in vitro* experiments and a comprehensive overview of its feature set compared to state-of-the-art devices in this field. Finally, section 4 summarizes the findings.

## 2 TECHNICAL REALIZATION

### 2.1 System Overview

STELLA+ utilizes a two-stacked PCB design in order to double available component area compared to a standard single PCB configuration (see Fig. 1 (b)).

The PCBs are stacked together using miniaturized connectors (Molex 505417-3410) allowing for the transfer of power and signals between the two boards. Fig. 1 (a) illustrates the system overview, highlighting the functional distribution between the PCBs.

The upper PCB is responsible for battery and power management, while also housing a Bluetooth Low Energy (BLE) module for wireless communication. It also includes a magnetic sensor for triggering basic device tasks and LEDs (red, green, IR) for status indication. Additionally, it incorporates sensory units, including a temperature sensor for monitoring the animal’s temperature and a circuit for characterizing the impedance of the electrode and tissue component over a broad spectrum (details not provided in this paper). On the other hand, the lower PCB focuses on the generation of charge-balanced DBS pulses for two channels, including an appropriate level translation to ensure compatibility between two voltage domains (see Section 2.2.3, 2.3.4). It also incorporates a built-in self-test to verify whether the electrical stimulation is within a valid range. Finally, it integrates a 3-axis accelerometer sensor for motion sensing of the animal.

### 2.2 Power Management

The power management of STELLA+ is conceptually presented in Fig. 2(a).

#### 2.2.1 Low-Power Approach

STELLA+ has been designed to be highly modular, allowing unused modules to be selectively powered down to the nA range via dedicated EN signals or the system bus. This approach permits the platform to be used in an energy-efficient fashion for each specific application. Furthermore, the platform utilizes two microcontrollers to effectively manage various

tasks. The nRF52833, which is built around a 32-bit ARM Cortex-M4, is used for computationally intensive tasks such as adaptive DBS algorithms. Additionally, the nRF52833 includes an RF transceiver module supporting Bluetooth Low Energy (BLE) for wireless communication with the outside world. In contrast, the MSP430FR2355 microcontroller, which features an ultra-low power architecture, is responsible for controlling and monitoring the stimulation signals.

### 2.2.2 Battery

The platform is powered by the rechargeable Li-ion button cell CP9440 A4X from VARTA (VARTA, 2019) providing a capacity of 29 mAh. With its compact dimensions of  $\varnothing 9.4 \times 4$  mm, and low weight of 0.9 g, this battery is highly suitable for applications with critical space.

### 2.2.3 Voltage Regulation

The previous STELLA implements a unified approach, where the control and stimulation unit share the same supply voltage generated by a boost converter. The boost converter was configured to convert the 3 V battery voltage into a system voltage of up to 3.7 V, allowing for a higher compliance voltage if needed. The unified approach offers the advantage of low circuit complexity, but achieves a low compliance voltage only due to low maximum tolerable supply voltage of the microcontroller and sensors. In STELLA+, a Li-ion battery (A4X) operating within a voltage range of 3 to 4.3 V is used as power source. In order to overcome the compliance voltage limitations of STELLA, a dual-VDD approach was applied, in which the control and stimulation unit was split into separate voltage domains. The control unit, including processors and sensors, is powered by an LDO (Low-Dropout) regulator (TPS7A0228) that provides a stable 2.8 V rail ( $V_{DD1}$ ). In contrast, the stimulation unit is connected to a flexible buck-boost converter topology. The boost (MAX17227A) and buck (MAX38642A) converter are single ICs with their outputs tied together. Each converter has an EN pin that is used to enable or disable the outputs. When disabled, the converter completely disconnects the load. The enable signal ( $EN_{DC/DC}$ ) is driven by the MSP430 and is routed directly to the boost converter and is inverted (74LVC1G04) for the buck converter. This configuration ensures that only one converter is active at any given time, preventing conflicting voltage outputs. The output voltage of each converter is controlled by an individual digital potentiometer (AD5142A) in rheostat mode via  $I^2C$ . This

topology enables the supply voltage for the stimulation unit ( $V_{DD2}$ ) to be scaled either above or below the battery voltage over a range of 2.5 V and 5.2 V. Combined with the built-in self-test (BIST) that identifies the maximum voltage at the end of the DBS pulse (see Section 2.3.7), this method enables energy-efficient adaptation of the supply voltage for the stimulation unit according to the load impedance requirements.

## 2.3 Stimulation Unit

The stimulation unit is presented conceptually in Fig. 2(a) and in detail in Fig. 2(c), while the level translation design is shown in Fig. 2(b).

### 2.3.1 Multi-Modal Architecture

STELLA+ features a multi-modal architecture capable of generating both charge-balanced current-controlled and charge-balanced voltage-controlled DBS pulses, both provided by clinical DBS devices. The MSP430 controls a 2:1 analog switch (TMUX1136) that enables the selection between the stimulation modes for each channel. The current-controlled mode is generally the preferred configuration, as it maintains a constant current regardless of load impedance changes (Kandadai et al., 2023; Hui et al., 2020; Lempka et al., 2010). Therefore, this mode is particularly optimized for energy efficiency and is the primary focus of this section. In view of current developments in other medical fields, such as traumatology, the voltage-controlled mode may also be suitable for other areas of application (Raben et al., 2024; Nicksic et al., 2022; Klinder et al., 2024). To this end, STELLA+ incorporates a 10-bit DAC (DAC6311) for each channel controlled by the SPI (Serial Peripheral Interface) bus, enabling the generation of any required voltage-driven waveform for the research objective. To ensure that only the AC component of the DAC signal, which is typically required in these application domains, contributes to the stimulation, a blocking capacitor is incorporated that forms a high-pass filter with the load. This capacitor is positioned behind the multiplexer to provide the current-controlled mode with a safety feature for the DBS application (see Section 2.3.7).

### 2.3.2 Generation of Current-Controlled DBS Pulses

The dual-channel design for generating current-driven DBS pulses builds on the previous STELLA architecture, utilizing an MSP430 microcontroller to precisely control the current amplitude, frequency and pulse width of the DBS pulses. The dual-channel

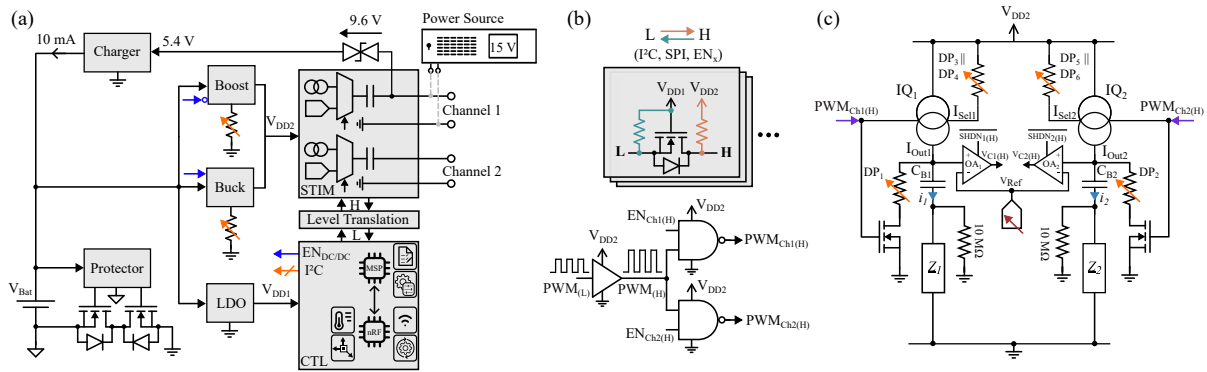


Figure 2: Architecture of STELLA+. (a) Block diagram illustrating the concept of battery and power management. (b) Level translation design. (c) Detailed circuitry of the stimulation unit for generating current-controlled and charge-balanced DBS pulses (adapted from (Plocksties et al., 2021a)).

capability is enabled by a dedicated constant current source (PSSI2021SAY) for each stimulation channel which allows the current amplitude to be adjusted individually. The assumption that a single current source's output will result in the half current amplitude by connecting the other microelectrode parallel to its output is invalid due to differing load impedances for each channel, as is the case in (Kölbl et al., 2016). The differences in load impedance are due to several factors, including the different conductivity values of white and grey matter (Gabriel and Gabriel, 1996; Hasgall et al., 2022; Koessler et al., 2017), the highly dynamic biological encapsulation processes that surround the electrodes after insertion (Evers et al., 2022; Lempka et al., 2009), and inherent manufacturing variations in the electrodes themselves (Payonk et al., 2025). Furthermore, it is not recommended to achieve a current-controlled stimulation by varying the resistor in series with a voltage source as is the case in (de Haas et al., 2012), or by adjusting the output voltage of a voltage source as is the case in (Liu et al., 2017). First, these approaches require frequent active readjustment due to the dynamic load, which might be energy-intensive. Second, the resulting current amplitudes can only be considered constant on a macroscopic time scale. At a microscopic level, the system still behaves like a voltage source, which cannot maintain a constant current during the pulse duration due to the capacitive component of the impedance load (see (de Haas et al., 2012)), resulting in only semi-current-controlled stimulation.

In STELLA+, both current sources ( $I_{Q1}, I_{Q2}$ ) are controlled by the MSP430's PWM (Pulse-width modulation) signal, that carries the frequency and pulse width information, resulting in synchronized DBS pulses for both channels. Similar to STELLA, the MSP430's clock in STELLA+ is sourced by an external 32,768 Hz crystal, thereby enabling the microcontroller to operate in ultra-low power mode. Con-

sequently, the pulse width and frequency can be adjusted in approximately  $30\mu\text{s}$  increments. In order to adjust the stimulation current of the previous STELLA, a digital potentiometer in rheostat mode in parallel with a fixed resistor is used to tailor the highly non-linear output of the current source with high resolution between  $50\mu\text{A}$  and  $100\mu\text{A}$ . However, if higher stimulation currents with high accuracy were required, the resistor had to be resoldered. In contrast, STELLA+ employs two digital potentiometers (AD5143) in parallel ( $DP_3 || DP_4, DP_5 || DP_6$ , all operating in rheostat mode) for adjusting the stimulation current of each channel, allowing high-resolution adjustments above  $100\mu\text{A}$  without the need for hardware modifications. Note that since the output current of the used current source varies with supply voltage, it must be calibrated across the entire supply voltage range. The same applies to temperature, requiring the output current to be calibrated under *in vivo* conditions.

### 2.3.3 Compliance Voltage

Most existing stimulation devices for rodents are designed for current-controlled stimulation, which ensures constant current delivery despite variations in load impedance (see Table 1). Maintaining a constant current requires sufficient compliance voltage to accommodate the diverse range of electrode configurations, stimulation parameters and electrode encapsulation caused by the biological response. In the existing literature on DBS devices, it is frequently assumed that the supply voltage of the current source is equal to the maximum voltage that the current source can provide for the load impedance. This assumption is incorrect, as the internal resistance of a current source leads to a voltage drop that reduces its maximum output voltage. This voltage drop varies depending on the type of current source, but is typ-



ically around 1 V. The current source's supply voltage minus the internal voltage drop is called compliance voltage. This consideration is especially important for DBS devices operating with a current source's supply voltage in the region of 3 V (Plocksties et al., 2021a; Fleischer et al., 2020; Grottemeyer et al., 2024; Fluri et al., 2017; Kouzani et al., 2017). While these devices typically feature a low current consumption, their relatively low compliance voltage below 3 V increases the risk that the constant current cannot be maintained within the pulse width when using standard stimulation protocols and standard electrodes. This can be especially critical when integrated monitoring capabilities are lacking to check whether the stimulation is in a valid range. In contrast, circuit designs that allow for higher compliance voltages result in significantly increased current consumption, even reaching the mA range in some cases (Ewing et al., 2013; Pinnell et al., 2018; Pinnell et al., 2015; Kölbl et al., 2016; Adams et al., 2019), which negatively impacts the ratio between battery volume and runtime. Furthermore, considering that typical rodent stimulation protocols use stimulation currents of no more than 100  $\mu$ A for 60  $\mu$ s (Reese et al., 2009; Evers et al., 2022; Leblois et al., 2010; Heerdegen et al., 2021; Paap et al., 2021; Zhang et al., 2024), devices operating at such high compliance voltages may be regarded as oversized and consequently inefficient. Using the bipolar microelectrode PI-SNEX-100 (Microprobes, Gaithersburg, USA), which is widely used in rodent DBS studies, our *ex vivo* voltage measurements in rodent brain tissue showed that the maximum voltage of the DBS pulse never exceeded 3.5 V for a 100  $\mu$ A/60  $\mu$ s pulse with a frequency of 130 Hz.

STELLA+ is designed for high energy efficiency to facilitate long-term experiments with a low battery volume while offering sufficient compliance voltage up to 4.3 V to support the most common stimulation setups in DBS research using rodent models (see Section 3.2, 3.3).

### 2.3.4 Level Translation

Given the 2.8 V operating voltage of the MSP430 and the up to 5.2 V domain of the stimulation unit in STELLA+, an appropriate level translation design is required that meets the requirements for ultra-low power consumption. In order to level-shift the low-voltage PWM signal ( $PWM_L$ ), which controls the rectangular stimulation pulses, to the higher voltage rail ( $PWM_H$ ), a translation buffer (74LV1T34) is used. Although the additional supply current in typical voltage translators increases significantly as the input voltages diverge from the supply voltage, this approach remains feasible due to very low duty cy-

cles encountered in DBS, such as a pulse width of 60  $\mu$ s and a frequency of 130 Hz. A dedicated IC is critical in this case as it ensures excellent signal integrity across the entire translation range required for the sharp rise and fall time of the rectangular waveform.

All other signals, including the I<sup>2</sup>C bus, SPI bus and EN signals, are level translated using n-channel MOSFETs (CSD15380F3) together with pull-up resistors, allowing reliable communication between the voltage domains. For unidirectional operation, low-to-high translation is achieved by a pull-up resistor at the high side, while high-to-low communication utilizes a pull-up at the low side. For bidirectional communication, as required by the I<sup>2</sup>C, pull-up resistors are implemented on both sides.

### 2.3.5 Charge Balancing

Any system designed for the electrical stimulation of tissue must keep the voltage across the working and counter electrode within the safe electrochemical window to avoid harmful byproducts to the surrounding tissue. Since biological tissue is mainly composed of water, exceeding a certain voltage threshold leads to the electrolysis of water (Boehler et al., 2020). This irreversible process can cause tissue damage due to the formation of oxygen and hydrogen gases, along with significant pH changes (Boehler et al., 2020; Huang et al., 2001). In the scenario of DBS, each stimulation pulse charges the double-layer capacitance that is formed at the electrode-tissue interface. It is critical to properly discharge this capacitance between pulses to prevent charge accumulation over time, ensuring that no sustained DC offset above the decomposition voltage of water can develop.

To address this, STELLA+ uses the established passive charge balancing method by connecting the stimulation electrode to ground through an adjustable resistor, similar to STELLA. However, this method has been slightly modified for STELLA+ by using a fast-switching n-channel MOSFET instead of an active switching IC, resulting in negligible power consumption of this method. This n-channel MOSFET is controlled by the high-voltage PWM signal for each channel ( $PWM_{Ch1(H)}$ ,  $PWM_{Ch2(H)}$ ). During the pulse-off phase, the MOSFET is activated, creating a discharge path for the double-layer capacitor. During the pulse-on phase, it enters the high impedance state, preventing interference with the stimulation pulse. The passive charge balancing approach induces a current reversal pulse. Without an additional resistor, the peak value of the reversal pulse depends on the DBS voltage and current value at the end of the pulse as well as the value of the electrolyte resistance (access

resistance). The larger the peak value, the more it could counteract the desired physiological effect of the stimulation impulse (Merrill et al., 2005). Therefore, a digital potentiometer (AD5143, 100 k $\Omega$ ) in rheostat mode is used in the discharge path of each channel to reduce this peak value ( $DP_1$ ,  $DP_2$ ). Note that the double-layer capacitor must be fully discharged before the next pulse is generated, as otherwise control over the electrode voltage will be lost. The time required for full discharge should include a sufficient safety margin to account for the various biological processes influencing the load impedance.

### 2.3.6 Independent Channel Control

While STELLA was developed for the simultaneous control of two channels, the new design offers the opportunity to activate or deactivate each DBS channel independently. This is achieved by connecting the high-voltage PWM signal ( $PWM_H$ ) to two NAND gates, with the other input of each gate connected to a level-shifted EN signal ( $EN_{Ch1(H)}$ ,  $EN_{Ch2(H)}$ ) controlled by the MSP430. This feature allows for reduced current consumption by deactivating the unused channel in unilateral operation, which is of special importance in unilateral disease models, e.g. the 6-hydroxydopamine model of Parkinson's disease (Ungerstedt, 1968). Furthermore, in the case of adaptive DBS (aDBS) it enables individual on-off control for both channels simply by switching the enable signals. The effectiveness of the on-off control scheme was demonstrated in the study by (Evers et al., 2024).

### 2.3.7 Safety and Reliability

The stimulation unit includes a DC blocking capacitor of 20  $\mu$ F placed in series with both current sources ( $C_{B1}$ ,  $C_{B2}$ ). This capacitor acts as a safety measure for the subject, preventing high faradaic currents if a sustained, high DC voltage occurs at the electrode in the event of a fault. However, it has been demonstrated that even when perfectly charge-balanced stimulation is applied, the blocking capacitor will generate an offset voltage at the electrode-tissue interface (van Dongen and Serdijn, 2016). To prevent the offset voltage potentially exceeding the water window, a high-ohmic resistance of 10 M $\Omega$  was placed in parallel to the load impedance for each channel. This allows an effective discharge path for the imbalanced charge, contributing to minimizing the offset voltage (see Section 3.2). Furthermore, the 10 M $\Omega$  resistor has a negligible impact on the stimulation current. For typical stimulation currents above 50  $\mu$ A that require the maximum current source's output voltage, this would result in a reduction of the stimulation current of only less than

1 %.

In DBS studies including rodents, typical defects such as shorted or open electrodes as well as an excessive load impedance are frequently encountered (Plocksties et al., 2021a; Plocksties et al., 2022). If these issues remain undetected, they can have a considerable impact on DBS experiments, as they have the potential to confound the experimental results and conclusions. Particularly when using backpacks or head-mounted DBS systems, the failure rate is considerable (Plocksties et al., 2021a). Therefore, it is crucial to integrate a method that reliably detects these problems. Similar to STELLA, STELLA+ incorporates a built-in self-test (BIST) that monitors and reports such issues. In a nutshell, the maximum voltage at the end of the DBS pulse is determined by gradually lowering the reference voltage at the inverting input of a comparator. As a slight improvement over the previous version, a dedicated 10-bit DAC (DAC6311) is used for generating the reference voltage ( $V_{Ref}$ ) via SPI instead of an 8-bit digital potentiometer, effectively increasing the accuracy of this measurement.

## 2.4 Battery Management

The circuitry of STELLA+ is designed for a rechargeable Li-ion battery as power source, replacing CR or SR button cells commonly used in existing rodent stimulators. This eliminates the need for frequent battery replacement. Additionally, the proposed circuit design enables recharging the battery directly via the electrode leads. This dual functionality is particularly advantageous for fully implantable stimulators, where the battery typically cannot be replaced or recharged without damaging the encapsulation. The battery management of STELLA+ is conceptually presented in Fig. 2(a).

### 2.4.1 Battery Protection

When using Li-ion batteries, following the safety protocols is essential, especially when implanted into living beings. Therefore, the circuit design has to contain adequate safety mechanisms to safeguard Li-ion batteries against overcharge, overdischarge, overcurrent and short-current. To address these safety requirements, we used a battery management IC (S-82A1ACA-I6T1U) in combination with two external n-channel MOSFETs resulting in disconnecting the GND potential if any value falls outside the valid range specified in the technical handbook from VARTA (VARTA, 2019). Falling below the overdischarge voltage of 3 V, this IC transitions to a power-down mode wherein it consumes 50 nA only, thus

preventing damage to the cell through continued discharge. A second layer of protection is provided by VARTA's vent holes integrated into the battery (VARTA, 2019). These vents ensure that any excess pressure is released to guarantee safety. For this, it must be ensured that the encapsulation of the device provides sufficient space for expansion.

#### 2.4.2 Battery Recharge

For recharging the A4X, a battery charger IC (BQ25100A) is used, configured with a charging limit of 4.3 V and a charge current of 10 mA. To allow the cable that transmits the stimulation signal to the electrode to also serve as a path for supplying power to the input of the charger IC, a bilateral TVS diode (SP0201B-ELC-01UTG) with a breakdown voltage of  $\pm 9.6$  V/1 mA is used. This low-capacitance diode prevents interference between the charger IC and the stimulation output. As the maximum voltage that the DBS pulse reaches is 4.3 V, this breakdown voltage is far below this value. Considering the voltage drop across the TVS diode with a charge current of 10 mA, the power source has to output approx. 15 V to provide a sufficiently high input voltage for the charger IC. A blocking capacitor in series to the current source ( $C_{B1}$ ), already used for protecting the brain tissue in a failure event, serves as high-voltage protection for the current source and the circuitry for the built-in self-test.

## 3 RESULTS AND DISCUSSION

### 3.1 Device Specifications

The PCBs are designed in a six-layer configuration with a high wiring density per unit area, enabling a small footprint despite a high IC package area. The manufactured boards measure 21x14.5 mm with a circular cut-out of 9.5 mm diameter to accommodate the battery for the overall system in a space-saving manner (see Fig. 3). When the PCBs are stacked, the total height is 4 mm, matching the height of the battery. The total PCB volume, calculated as 21x14.5x4 mm minus the volume of the cut-out, results in 935 mm<sup>3</sup>. The PCB weight is 1.2 g, while the complete device including the battery weighs 2.1 g. When combined with the reliable and compact encapsulation method presented in (Plocksties et al., 2021b), for example, the device specifications might be highly suitable for fully subcutaneous implantation in small rodents.

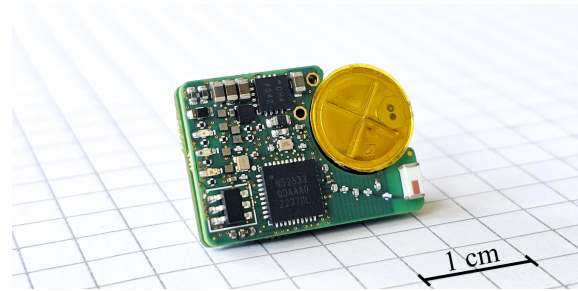


Figure 3: STELLA+ demonstrated on graph paper, featuring the PCB stack and Li-ion battery.

### 3.2 In Vitro Characterization of the Stimulation Unit

#### 3.2.1 Measurement Setup

The performance of the stimulation unit of STELLA+ for current-controlled DBS was evaluated in an *in vitro* setting. A PI-SNEX-100 microelectrode was connected to one channel of STELLA+ and immersed in a NaCl conductivity standard solution of  $0.199 \pm 0.002$  S m<sup>-1</sup> at 25 °C. This conductivity was chosen because it lies within the range of reported conductivity values for white and grey matter (Gabriel and Gabriel, 1996; Hasgall et al., 2022; Koessler et al., 2017; Akhtari et al., 2006), considering the relevant frequency range derived from the frequency spectrum of the DBS signal (Badstuebner et al., 2017; Gimsa et al., 2005).

For the measurements presented in Fig. 4(a)-(c), the current amplitude was increased by 50  $\mu$ A and the pulse width was increased by 30  $\mu$ s simultaneously, starting with 50  $\mu$ A/60  $\mu$ s and ending with 200  $\mu$ A/150  $\mu$ s. The frequency was set to 130 Hz for all settings. For the measurement presented in Fig. 4(d), STELLA+ was programmed to a random on-off sequence of current-controlled DBS pulses with a stimulation set to 100  $\mu$ A, 60  $\mu$ s and 130 Hz. For all stimulation settings, passive charge balancing is conducted with a minimal resistance in the discharge path (in the lower hundreds  $\Omega$ -range), which can be neglected since the electrolyte resistance is much higher in this case. The change in stimulation parameters was initiated by a magnet that triggered the magnetic sensor. Current and voltage recordings were performed using the CX3324A waveform analyzer with a sample rate of 10 MSa/s.

The voltage measurements were conducted by connecting the probe tip to the channel output and the probe ground lead to ground. Current measurements were taken by placing the current probe in series, with the positive terminal connected to the channel output and the negative terminal to the load. In this setup, the

stimulation pulses are recorded in the positive range, in contrast to the negative range in which the signals are usually presented in the literature as an indication of the commonly used cathodic stimulation. The representation in the positive range is only intended for clearer visualization of the signals in an ‘upright’ format and is not related to the polarity of the electrode contacts.

Furthermore, the voltage recordings were performed using a high-speed operational amplifier with a high input impedance (OPA810,  $12\text{ G}\Omega||2\text{ pF}$  in common mode) in a unity-gain buffer configuration. This setup is required especially for the offset voltage measurements presented in Fig. 4(c) because the relatively low input resistance of 1 or  $10\text{ M}\Omega$  for a typical probe would otherwise have provided an external discharge path for the accumulated charge, which would have distorted the offset voltage results.

### 3.2.2 Results

The voltage recordings in Fig. 4(a) exhibited the characteristic waveform associated with current-controlled stimulation. The voltage increases rapidly initially, representing the voltage drop across the electrolyte resistance, and is followed by the voltage drop across the electrode-electrolyte interface (Boehler et al., 2020). No offset voltage can be observed in the volt range. Only a closer examination in the millivolt range reveals its presence (see Fig. 4(c)).

The current recordings in Fig. 4(b) demonstrated sharp rising and falling edges, as well as a precise constant current throughout the pulse width across all settings. The end of each pulse is followed by the reversal pulse that results from shorting the electrode to ground. Without the use of an additional resistor in the discharge path, the reversal pulses show peak values that have slightly higher magnitudes than the stimulation current, with a maximum of approx.  $100\text{ }\mu\text{A}$ . After the peak, the current drops exponentially, with the double-layer capacitor almost completely discharged after five time constants, which are reached in less than one millisecond for all settings. For typical stimulation frequencies, this short discharge time enables the use of a resistance in the discharge path in order to reduce the peak value of the reversal pulse to at least the same magnitude as the stimulation current, a value commonly used in active charge balancing (symmetric biphasic) (Parastarfeizabadi and Kouzani, 2017).

The voltage recordings presented in Fig. 4(c) indicate the offset voltage caused by the blocking capacitor. After the start of stimulation, the offset voltage shifted towards more negative values over time and the observations were continued until stabiliza-

tion, which occurred after approximately 5 minutes. The figure shows the offset voltage in the steady state between two DBS pulses for each stimulation parameter setting. This offset can be approximated as consistent DC bias, as the DBS pulse is short relative to the pulse-off phase and the offset voltage reaches its value rapidly after the DBS pulse. Furthermore, the figure shows that the magnitude of the offset voltage increases with higher injected charge, which is explained in (van Dongen and Serdijn, 2016). For the  $50\text{ }\mu\text{A}/60\text{ }\mu\text{s}$  pulse, the offset voltage is recorded as the smallest negative value at  $-25\text{ mV}$ , whereas the  $200\text{ }\mu\text{A}/150\text{ }\mu\text{s}$  pulse results in the most negative offset voltage of  $-70\text{ mV}$ . Considering the theoretical minimum potential difference of  $1.23\text{ V}$  needed for water splitting (Lamy and Millet, 2020) as the critical limit for the developed DC bias absolute value, the measured offset voltages are significantly lower for all settings. This high safety margin is achieved by the integrated  $10\text{ M}\Omega$  resistor in parallel to the load, which provides an effective discharge path for the imbalanced charge.

The Fig. 4(d) presents a randomly timed DBS on-off scheme. The stimulation pulses show a precise stimulation current of  $100\text{ }\mu\text{A}$ , accompanied by the reversal pulses resulting from the charge balancing method. The on-off pattern is achieved by toggling the enable signal ( $\text{EN}_{\text{Ch1(H)}}$ ) at the input of the AND gate of the first channel. Moreover, the enable signal switches between  $0\text{ V}$  and  $4\text{ V}$ , demonstrating the proper functioning of the level translation (see Section 2.3.4). The measurements show that STELLA+ effectively enables the implementation of this aDBS control option.

## 3.3 Current Consumption vs. Compliance Voltage

The compliance voltage and corresponding current consumption are important performance metrics for a neurostimulator that delivers current-controlled stimulation pulses. To investigate this relationship for STELLA+, the following measurement setup was designed.

### 3.3.1 Measurement Setup

The current waveform analyzer CX3324A was placed in series with an external power supply and STELLA+. The power supply was set to  $3.7\text{ V}$ , which is the nominal voltage of the A4X series. The current consumption was then measured for the supply voltage at a minimum of  $2.5\text{ V}$  and a maximum of  $5.2\text{ V}$  provided by the buck-boost topology. The CX3324A



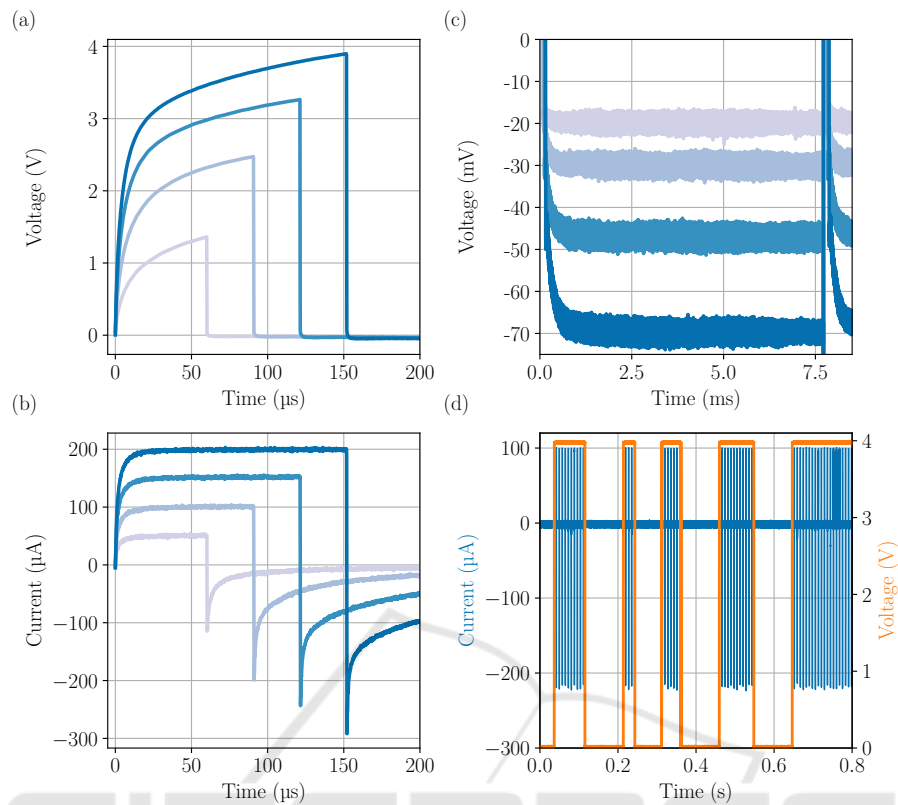


Figure 4: Performance of STELLA+ in delivering current-controlled stimulation pulses via a bipolar PI-SNEX-100 immersed in a  $0.199 \text{ S m}^{-1}$  saline solution. The figure illustrates recordings of (a) voltage and (b) current of the DBS pulse, as well as (c) the offset voltage in steady state at various stimulation parameters: —  $50 \mu\text{A}/60 \mu\text{s}$ , —  $100 \mu\text{A}/90 \mu\text{s}$ , —  $150 \mu\text{A}/120 \mu\text{s}$ , —  $200 \mu\text{A}/150 \mu\text{s}$ , all at a frequency of 130 Hz. Additionally, (d) a randomly timed DBS on-off scheme controlled by the enable signal (—) is shown, with stimulation set to  $100 \mu\text{A}$ ,  $60 \mu\text{s}$  and 130 Hz (—).

sampled the current at 1 MSa/s and the final result was calculated by averaging the measurement over a period of 20 s. Furthermore, both measurements were performed in DBS-on mode, using the following stimulation parameters: bilateral stimulation with a load of  $10 \text{ k}\Omega$  respectively,  $100 \mu\text{A}$  current amplitude,  $60 \mu\text{s}$  pulse width and 130 Hz frequency. Finally, the compliance voltage was determined as the voltage at which the adjusted constant current started to drop, which was observed with an oscilloscope. This was typically noticed when the voltage of the DBS pulse exceeded the level that was  $0.9 \text{ V}$  lower than the current source's supply voltage.

### 3.3.2 Results

STELLA+ achieves at its minimum compliance voltage of  $1.6 \text{ V}$  a current consumption of  $8.9 \mu\text{A}$  and at its maximum compliance voltage of  $4.3 \text{ V}$  a current consumption of  $25.1 \mu\text{A}$ . In comparison, the previous STELLA version achieved a maximum compliance voltage of  $2.8 \text{ V}$  with  $12.2 \mu\text{A}$ .

The results show that STELLA+ provides a higher compliance voltage than its predecessor, enabling a wider range of stimulation setups while still maintaining an ultra-low current consumption for long-term studies. When the maximum compliance voltage is required, STELLA+ still provides 6.8 weeks of stimulation using the CP9440 A4X battery (29 mAh), which is sufficient for most rodent DBS studies.

## 3.4 Comparison of Features with the State-of-the-Art

To compare the results with other DBS devices designed for rodent studies, a review of the relevant literature was conducted. ASIC designs were excluded from the comparison due to their specialized and proprietary nature, e.g. (Arfin et al., 2009). In contrast, DBS devices using off-the-shelf discrete components allow the research community to replicate the designs and customize them to their experimental needs.

Table 1 presents the feature set of existing rodent DBS devices, organized by publication year

Table 1: Comparison of key features in existing rodent DBS devices designed with off-the-shelf components.

DBS device	PCB Volume category	Device control	Data output technology	Provided device/physiological data	Device Mounting	Stimulation properties	Extra features
		Radio frequency (RF) Physical switch/potentiometer Reed switch/Magnetic sensors	Optical Radio frequency (RF)	High-accuracy temperature Local field potentials (LFPs) Load impedance (OOR) Battery voltage (OOR) Stimulation on/off	Implant Back Head	Dual-channel Current-controlled Voltage-controlled Charge-balanced Adaptive DBS capabilities	On-board battery recharge Auto-set compliance voltage SW-adjustable stim. parameters
<b>Battery-powered</b>							
STELLA+	L	● ● - -	● ●	● ● ● ● ● ●	- - - - ●	● ● ● ● ● ●	● ● ●
Grottemeyer2024	VL	● ● - -	● ●	● ● ● ● ● ●	- - - - ●	● ● ● ● ● ●	● ● ●
STELLA2021	VL	- - - -	● *	● ● ● ● ● ●	- - - - ●	● ● ● ● ● ●	● ● ●
Tala2021	H	● ● - -	● ●	● ● ● ● ● ●	- - - - ●	● ● ● ● ● ●	● ● ●
Fleischer2020	VL	● ● - -	● ●	● ● ● ● ● ●	- - - - ●	● ● ● ● ● ●	● ● ●
Adams2019	M	- - - -	● ●	● ● ● ● ● ●	- - - - ●	● ● ● ● ● ●	● ● ●
Alpaugh2019	M	- - - -	● ●	● ● ● ● ● ●	- - - - ●	● ● ● ● ● ●	● ● ●
Schulz2019	M	- - - -	● ●	● ● ● ● ● ●	- - - - ●	● ● ● ● ● ●	● ● ●
Pinnell2018	L	● ● - -	● ●	● ● ● ● ● ●	- - - - ●	● ● ● ● ● ●	● ● ●
Fluri2017	M	- - - -	● ●	● ● ● ● ● ●	- - - - ●	● ● ● ● ● ●	● ● ●
Liu2017	M	● ● - -	● ●	● ● ● ● ● ●	- - - - ●	● ● ● ● ● ●	● ● ●
Kouzani2017	L	● ● - -	● ●	● ● ● ● ● ●	- - - - ●	● ● ● ● ● ●	● ● ●
Parastarfeizabadi2016	VL	- - - -	● ●	● ● ● ● ● ●	- - - - ●	● ● ● ● ● ●	● ● ●
Kölbl2016	L	- - - -	● ●	● ● ● ● ● ●	- - - - ●	● ● ● ● ● ●	● ● ●
Pinnell2015	M	● ● - -	● ●	● ● ● ● ● ●	- - - - ●	● ● ● ● ● ●	● ● ●
Acosta2015	VL	- - - -	● ●	● ● ● ● ● ●	- - - - ●	● ● ● ● ● ●	● ● ●
Hentall2013	L	- - - -	● ●	● ● ● ● ● ●	- - - - ●	● ● ● ● ● ●	● ● ●
Ewing2013	M	● ● - -	● ●	● ● ● ● ● ●	- - - - ●	● ● ● ● ● ●	● ● ●
Haas2012	L	- - - -	● ●	● ● ● ● ● ●	- - - - ●	● ● ● ● ● ●	● ● ●
Forni2012	L	- - - -	● ●	● ● ● ● ● ●	- - - - ●	● ● ● ● ● ●	● ● ●
Harnack2008	M	● ● - -	● ●	● ● ● ● ● ●	- - - - ●	● ● ● ● ● ●	● ● ●
<b>Battery-free (Wireless power transfer)</b>							
Burton2021	VL	● ● - -	● ●	● ● ● ● ● ●	- - - - ●	● ● ● ● ● ●	● ● ●
Heo2015	M	● ● - -	● ●	● ● ● ● ● ●	- - - - ●	● ● ● ● ● ●	● ● ●
Millard2007	L	● ● - -	● ●	● ● ● ● ● ●	- - - - ●	● ● ● ● ● ●	● ● ●

● = Feature is implemented; ● = Feature is partially implemented; - = Feature is not implemented; ♦ = Out of range indication; \* = Optical wireless communication provided (for STELLA2021 refer to (Koschay et al., 2022)); h = Inadequate current source design (see 2.3.2); ^ = Inadequate dual-channel design (see 2.3.2); # = Constant current adjustment manually via potentiometer; † = Partial subcutaneous implant only;  
 VL: Very Low (< 500 mm<sup>3</sup>), L: Low (500 – 1000mm<sup>3</sup>), M: Medium (1000 – 5000mm<sup>3</sup>), H: High (> 5000 mm<sup>3</sup>)

and divided into two classes: battery-powered and battery-free. Battery-powered devices operate by using batteries, while battery-free devices depend solely on wireless power transfer (WPT) from an external source. Note that WPT requires specialized cages that can lead to unreliable operation if coils are misaligned due to the animal movement, and prevent essential behavioral experiments like the Morris water maze (Millard and Shepherd, 2007; Burton et al., 2021; Evers et al., 2022).

The features identified in the literature were organized into categories, which are analyzed in the following.

**PCB Volume Category:** The PCB volume is of crucial importance as it dictates the mounting options and overall impact on the animal. The DBS devices were categorized based on their PCB volume into four classes (see Table 1). In cases where the PCB volume was not indicated, it was estimated from the photo-

graphic scale. The volume specifications are based on earlier work and were expanded in this study by further DBS devices (Plocksties et al., 2021a).

STELLA+ falls into the ‘low’ category as it has been specifically designed to allow fully subcutaneous implantation in small rodents.

**Device Control:** Radio frequency communication is considered the most effective control method as it allows to modify a wide range of device parameters without disturbing the animal. However, the requirement for considerable PCB area, the need for higher power consumption and the complexity of RF design have limited its widespread use. The most commonly used control method involves magnetic sensors, which are mainly used to trigger specific device functions, such as integrated self-tests. Some stimulators also incorporate physical elements, including switches and potentiometers. However, these components are large as they have to be operated manually,

leading to a poor functionality-to-size ratio. Another control mechanism involves transmitting light pulses to a photodiode. However, this approach is challenging due to the movement of the animals and is currently only used in one stimulator (Heo et al., 2015).

In contrast, STELLA+ does not include any optical or physical elements for its control. Instead, it uses Bluetooth Low Energy (BLE), which enables detailed configuration of the device parameters from a great distance to the animal. To ensure redundancy, the device includes a magnetic sensor for essential tasks, like turning the stimulation on/off.

**Data Output Technology:** RF communication enables high data rates, which are required for the wireless transmission of physiological data, such as local field potentials and accelerometer data. However, due to the aforementioned obstacles associated with RF modules, optical data transmission is most commonly used in DBS devices. For this, LEDs are utilized that operate either in the visible spectrum or in the infrared range (IR), with simple blinking patterns indicating device information, e.g. low battery voltage alerts.

STELLA+ employs the nRF52833 microcontroller, which supports BLE for efficient transmission of device and physiological data. Additionally, STELLA+ features two visible LEDs (red and green) and an IR LED for convenient indication of device information.

**Provided Device/Physiological Data:** Most DBS devices provide only basic device-specific data, such as low battery voltage alerts and the stimulation status (on/off). However, the indication of out-of-range load impedance is rarely provided, despite its significance for replicable experiments. In addition, only two DBS devices allow the transmission of the applied stimulation protocol, which is important for verifying that the stimulation parameters are set correctly, especially when they have been changed. Moreover, only one device is able to transmit physiological data wirelessly, specifically local field potentials (LFPs) (Pinnell et al., 2015). The other device that enables the readout of LFPs, processes this data entirely on-board (Parastarfeizabadi et al., 2016).

STELLA+ is the first DBS device for rodents that incorporates a high-accuracy temperature sensor and a 3-axis accelerometer. The accelerometer enables the investigation of movement profiles, which could represent a potential biomarker for adaptive DBS, while requiring significantly less PCB area and energy compared to traditional LFP recordings. Additionally, STELLA+ provides data on the battery voltage, the on/off status of the stimulation, the applied stimulation protocol, and whether the load impedance is within a valid range. All device and physiological

data can be transmitted wirelessly via BLE.

**Device Mounting:** Most DBS devices are designed for head or backpack mounting, which limits animal mobility and often leads to higher failure rates. Fully implantable stimulators overcome these problems, but are more challenging to realize due to their high degree of miniaturization and waterproof encapsulation.

STELLA+ is characterized by a small stimulator-battery volume, making it ideal for subcutaneous implantation in small rodents. Its flat profile also supports the healing process by reducing tension on the overlying skin.

**Stimulation Properties:** Most DBS devices are primarily designed with charge-balanced current-controlled stimulation, while voltage-controlled stimulation is rarely implemented. Furthermore, the majority of DBS devices are designed for single-channel stimulation, which limits DBS to one hemisphere. A dual-channel design is less common, although a second channel is essential for studying bilateral DBS.

In contrast, STELLA+ provides the ability to select between charge-balanced current-controlled and charge-balanced voltage-controlled stimulation for one or two channels. Moreover, STELLA+ features aDBS capabilities through on-off switching of stimulation based on feedback data from a 3-axis accelerometer. This functionality is only supported by two other stimulators, which differ in that they use LFPs as feedback data (Pinnell et al., 2015; Parastarfeizabadi et al., 2016). Additionally, STELLA+ includes a powerful processing core that enables on-board processing capabilities for complex algorithms.

**Extra Features:** DBS devices often provide the extra feature of adjusting the stimulation parameters current amplitude, frequency and pulse width via software. In cases where this feature is only partially available, the adjustment of the current amplitude is typically limited to the use of an analog potentiometer or the resoldering of a resistor.

With STELLA+, all stimulation parameters can be configured via software and also adjusted wirelessly via BLE during the experiment. Additionally, the automatic adjustment of the compliance voltage improves energy efficiency and is exclusive to both STELLA+ and its predecessor. Finally, STELLA+ supports on-board battery recharging via electrode leads, an extra feature that is also present in only one other DBS device via wireless power transfer.

In summary, it can be concluded from Table 1 that STELLA+ has a wider and unique feature set compared with other state-of-the-art DBS devices for rodent DBS.

## 4 CONCLUSION

We introduce STELLA+, an innovative research platform designed for advanced DBS studies in freely-moving rodents. This paper serves as a starting point for future *in vivo* DBS studies in rodents and primarily focuses on the specifications and capabilities of STELLA+. The initial results highlight STELLA+'s compact design, energy-efficient architecture, integrated system monitoring and accurate generation of current-controlled and charge-balanced DBS pulses, which together form the basis for effective preclinical DBS research. Equipped with multiple sensors, a powerful processing unit and a Bluetooth Low Energy module, STELLA+ enables research into closed-loop stimulation. Compared to its predecessor and other state-of-the-art DBS devices, STELLA+ offers unprecedented experimental flexibility (see Table 1), rendering it an essential tool for both traditional and adaptive DBS research in rodents.

## ACKNOWLEDGMENT

Funded by the Deutsche Forschungsgemeinschaft (DFG, German Research Foundation) - SFB 1270/1,2 - 299150580. Our special thanks go to VARTA for providing Li-ion button cells for research purposes and to Uwe Knüpfer for his manufacturing support.

## REFERENCES

- Adams, S. D., Bennet, K. E., Tye, S. J., Berk, M., and Kouzani, A. Z. (2019). Development of a miniature device for emerging deep brain stimulation paradigms. *PLOS ONE*, 14(2):e0212554.
- Akhtari, M., Salamon, N., Duncan, R., Fried, I., and Mathern, G. (2006). Electrical conductivities of the freshly excised cerebral cortex in epilepsy surgery patients; correlation with pathology, seizure duration, and diffusion tensor imaging. *Brain Topography*, 18:281–290.
- Arfin, S. K., Long, M. A., Fee, M. S., and Sarpeshkar, R. (2009). Wireless neural stimulation in freely behaving small animals. *Journal of neurophysiology*, 102(1):598–605.
- Badstuebner, K., Gimsa, U., Weber, I., Tuchscherer, A., and Gimsa, J. (2017). Deep brain stimulation of hemiparkinsonian rats with unipolar and bipolar electrodes for up to 6 weeks: Behavioral testing of freely moving animals. *Parkinson's Disease*, 2017:1–18.
- Boehler, C., Carli, S., Fadiga, L., Stieglitz, T., and Asplund, M. (2020). Tutorial: guidelines for standardized performance tests for electrodes intended for neural interfaces and bioelectronics. *Nature protocols*, 15(11):3557–3578.
- Burton, A., Won, S. M., Sohrabi, A. K., Stuart, T., Amirhossein, A., Kim, J. U., Park, Y., Gabros, A., Rogers, J. A., Vitale, F., et al. (2021). Wireless, battery-free, and fully implantable electrical neurostimulation in freely moving rodents. *Microsystems & nanoengineering*, 7(1):62.
- de Haas, R., Struikmans, R., van der Plasse, G., van Kerkhof, L., Brakkee, J. H., Kas, M. J., and Westenberg, H. G. (2012). Wireless implantable microstimulation device for high frequency bilateral deep brain stimulation in freely moving mice. *Journal of neuroscience methods*, 209(1):113–119.
- Díez-Solinska, A., Vegas, O., and Azkona, G. (2022). Refinement in the european union: a systematic review. *Animals*, 12(23):3263.
- Evers, J., Orłowski, J., Jahns, H., and Lowery, M. M. (2024). On-off and proportional closed-loop adaptive deep brain stimulation reduces motor symptoms in freely moving hemiparkinsonian rats. *Neuromodulation: Technology at the Neural Interface*, 27(3):476–488.
- Evers, J., Sridhar, K., Liegey, J., Brady, J., Jahns, H., and Lowery, M. (2022). Stimulation-induced changes at the electrode–tissue interface and their influence on deep brain stimulation. *Journal of Neural Engineering*, 19(4):046004.
- Ewing, S. G., Lipski, W. J., Grace, A. A., and Winter, C. (2013). An inexpensive, charge-balanced rodent deep brain stimulation device: A step-by-step guide to its procurement and construction. *Journal of Neuroscience Methods*, 219(2):324–330.
- Fleischer, M., Endres, H., Sendtner, M., and Volkmann, J. (2020). Development of a fully implantable stimulator for deep brain stimulation in mice. *Frontiers in Neuroscience*, 14.
- Fluri, F., Mützel, T., Schuhmann, M. K., Krstić, M., Endres, H., and Volkmann, J. (2017). Development of a head-mounted wireless microstimulator for deep brain stimulation in rats. *Journal of Neuroscience Methods*, 291:249–256.
- Forni, C., Mainard, O., Melon, C., Goguenheim, D., Goff, L. K.-L., and Salin, P. (2012). Portable microstimulator for chronic deep brain stimulation in freely moving rats. *Journal of Neuroscience Methods*, 209(1):50–57.
- Gabriel, C. and Gabriel, S. (1996). Compilation of the dielectric properties of body tissues at rf and microwave frequencies.
- Gimsa, J., Habel, B., Schreiber, U., van Rienen, U., Strauss, U., and Gimsa, U. (2005). Choosing electrodes for deep brain stimulation experiments—electrochemical considerations. *Journal of Neuroscience Methods*, 142(2):251–265.
- Grottemeyer, A., Petschner, T., Peach, R., Hoehl, D., Knauer, T., Thomas, U., Endres, H., Blum, R., Sendtner, M., Volkmann, J., and Ip, C. W. (2024). Standardized wireless deep brain stimulation system for mice. *npj Parkinson's Disease*, 10(1).



- Hamani, C. and Nóbrega, J. N. (2010). Deep brain stimulation in clinical trials and animal models of depression. *European Journal of Neuroscience*, 32(7):1109–1117.
- Harmesen, I. E., Elias, G. J., Beyn, M. E., Boutet, A., Pancholi, A., Germann, J., Mansouri, A., Lozano, C. S., and Lozano, A. M. (2020). Clinical trials for deep brain stimulation: Current state of affairs. *Brain Stimulation*, 13(2):378–385.
- Hasgall, P., Di Gennaro, F., Baumgartner, C., Neufeld, E., Lloyd, B., Gosselin, M., Payne, D., Klingenböck, A., and Kuster, N. (2022). It's database for thermal and electromagnetic parameters of biological tissues, version 4.1.
- Heerdegen, M., Zwar, M., Franz, D., Hörnschemeyer, M. F., Neubert, V., Plocksties, F., Niemann, C., Timmermann, D., Bahls, C., van Rienen, U., et al. (2021). Mechanisms of pallidal deep brain stimulation: Alteration of cortico-striatal synaptic communication in a dystonia animal model. *Neurobiology of Disease*, 154:105341.
- Heo, M. S., Moon, H. S., Kim, H. C., Park, H. W., Lim, Y. H., and Paek, S. H. (2015). Fully implantable deep brain stimulation system with wireless power transmission for long-term use in rodent models of parkinson's disease. *Journal of Korean Neurosurgical Society*, 57(3):152–158.
- Huang, C. Q., Carter, P. M., and Shepherd, R. K. (2001). Stimulus induced pH changes in cochlear implants: an in vitro and in vivo study. *Annals of biomedical engineering*, 29:791–802.
- Hui, D., Murgai, A. A., Gilmore, G., Mohideen, S. I., Parent, A. G., and Jog, M. S. (2020). Assessing the effect of current steering on the total electrical energy delivered and ambulation in parkinson's disease. *Scientific Reports*, 10(1):8256.
- Jakobs, M., Fomenko, A., Lozano, A. M., and Kiening, K. L. (2019). Cellular, molecular, and clinical mechanisms of action of deep brain stimulation—a systematic review on established indications and outlook on future developments. *EMBO molecular medicine*, 11(4):e9575.
- Kandadai, R. M., Meka, S. S., Kola, S., Alugolu, R., and Borgohain, R. (2023). Constant current versus constant voltage dbs stimulators—changing trend. *Annals of Indian Academy of Neurology*, 26(4):368–369.
- Klinder, A., Moews, F., Ziebart, J., Su, Y., Gabler, C., Jonitz-Heincke, A., van Rienen, U., Ellenrieder, M., and Bader, R. (2024). Effects of electrical stimulation with alternating fields on the osseointegration of titanium implants in the rabbit tibia—a pilot study. *Frontiers in Bioengineering and Biotechnology*, 12:1395715.
- Koessler, L., Colnat-Coulbois, S., Cecchin, T., Hofmanis, J., Dmochowski, J. P., Norcia, A. M., and Maillard, L. G. (2017). In-vivo measurements of human brain tissue conductivity using focal electrical current injection through intracerebral multicontact electrodes. *Human brain mapping*, 38(2):974–986.
- Koschay, M., Richter, H., Statz, M., Kober, M., Puschmann, J., Plocksties, F., Storch, A., Kühn, V., and Timmermann, D. (2022). Case-study on visible light communication for implant monitoring. In *2022 IEEE Biomedical Circuits and Systems Conference (BioCAS)*, pages 275–279. IEEE.
- Kouzani, A. Z., Kale, R. P., Zarate-Garza, P. P., Berk, M., Walder, K., and Tye, S. J. (2017). Validation of a portable low-power deep brain stimulation device through anxiolytic effects in a laboratory rat model. *IEEE Transactions on Neural Systems and Rehabilitation Engineering*, 25(9):1365–1374.
- Kölbl, F., N'Kaoua, G., Naudet, F., Berthier, F., Faggiani, E., Renaud, S., Benazzouz, A., and Lewis, N. (2016). An embedded deep brain stimulator for biphasic chronic experiments in freely moving rodents. *IEEE Transactions on Biomedical Circuits and Systems*, 10(1):72–84.
- Lamy, C. and Millet, P. (2020). A critical review on the definitions used to calculate the energy efficiency coefficients of water electrolysis cells working under near ambient temperature conditions. *Journal of power sources*, 447:227350.
- Leblois, A., Reese, R., Labarre, D., Hamann, M., Richter, A., Boraud, T., and Meissner, W. G. (2010). Deep brain stimulation changes basal ganglia output nuclei firing pattern in the dystonic hamster. *Neurobiology of disease*, 38(2):288–298.
- Lempka, S. F., Johnson, M. D., Miocinovic, S., Vitek, J. L., and McIntyre, C. C. (2010). Current-controlled deep brain stimulation reduces in vivo voltage fluctuations observed during voltage-controlled stimulation. *Clinical Neurophysiology*, 121(12):2128–2133.
- Lempka, S. F., Miocinovic, S., Johnson, M. D., Vitek, J. L., and McIntyre, C. C. (2009). In vivo impedance spectroscopy of deep brain stimulation electrodes. *Journal of neural engineering*, 6(4):046001.
- Liu, H., Wang, C., Zhang, F., and Jia, H. (2017). An implantable device for neuropsychiatric rehabilitation by chronic deep brain stimulation in freely moving rats. *NeuroReport*, 28(3):128–133.
- Merrill, D. R., Bikson, M., and Jefferys, J. G. (2005). Electrical stimulation of excitable tissue: design of efficacious and safe protocols. *Journal of neuroscience methods*, 141(2):171–198.
- Millard, R. E. and Shepherd, R. K. (2007). A fully implantable stimulator for use in small laboratory animals. *Journal of neuroscience methods*, 166(2):168–177.
- Neumann, W.-J., Gilron, R., Little, S., and Tinkhauser, G. (2023). Adaptive deep brain stimulation: From experimental evidence toward practical implementation. *Movement disorders*, 38(6):937–948.
- Nicksic, P. J., Donnelly, D. T., Verma, N., Setiz, A. J., Shoffstall, A. J., Ludwig, K. A., Dingle, A. M., and Poore, S. O. (2022). Electrical stimulation of acute fractures: A narrative review of stimulation protocols and device specifications. *Frontiers in Bioengineering and Biotechnology*, 10:879187.
- Paap, M., Perl, S., Lüttig, A., Plocksties, F., Niemann, C., Timmermann, D., Bahls, C., van Rienen, U., Franz, D., Zwar, M., Rohde, M., Köhling, R., and Richter, A. (2021). Deep brain stimulation by optimized stimulators in a phenotypic model of dystonia: Effects

- of different frequencies. *Neurobiology of Disease*, 147:105163.
- Parastarfeizabadi, M. and Kouzani, A. Z. (2017). Advances in closed-loop deep brain stimulation devices. *Journal of neuroengineering and rehabilitation*, 14:1–20.
- Parastarfeizabadi, M., Kouzani, A. Z., Gibson, I., and Tye, S. J. (2016). A miniature closed-loop deep brain stimulation device. In *2016 38th Annual International Conference of the IEEE Engineering in Medicine and Biology Society (EMBC)*, pages 1786–1789. IEEE.
- Payonk, J. P., Bathel, H., Arbeiter, N., Kober, M., Fauser, M., Storch, A., van Rienen, U., and Zimmermann, J. (2025). Improving computational models of deep brain stimulation through experimental calibration. *Journal of neuroscience methods*, 414:110320.
- Pinnell, R., Dempster, J., and Pratt, J. (2015). Miniature wireless recording and stimulation system for rodent behavioural testing. *Journal of neural engineering*, 12(6):066015.
- Pinnell, R. C., de Vasconcelos, A. P., Cassel, J. C., and Hofmann, U. G. (2018). A miniaturized, programmable deep-brain stimulator for group-housing and water maze use. *Frontiers in Neuroscience*, 12.
- Plocksties, F., Kober, M., Niemann, C., Heller, J., Fauser, M., Nüssel, M., Uster, F., Franz, D., Zwar, M., Lüttig, A., Kröger, J., Harloff, J., Schulz, A., Richter, A., Köhling, R., Timmermann, D., and Storch, A. (2021a). The software defined implantable modular platform (STELLA) for preclinical deep brain stimulation research in rodents. *Journal of Neural Engineering*, 18(5):056032.
- Plocksties, F., Lüttig, A., Niemann, C., Uster, F., Franz, D., Kober, M., Koschay, M., Perl, S., Richter, A., Köhling, R., et al. (2022). Strategies on deep brain stimulation devices for effective behavioral studies in rodents. In *2022 IEEE-EMBS Conference on Biomedical Engineering and Sciences (IECBES)*, pages 376–381. IEEE.
- Plocksties, F., Shah, O. U., Uster, F., Ali, M., Koschay, M., Kober, M., Storch, A., and Timmermann, D. (2021b). Energy-efficient modular RF interface for fully implantable electrical devices in small rodents. In *2021 IEEE Biomedical Circuits and Systems Conference (BioCAS)*. IEEE.
- Raben, H., Kämmerer, P. W., and van Rienen, U. (2024). Addressing model uncertainties in finite element simulation of electrically stimulated implants for critical-size mandibular defects. *IEEE Transactions on Biomedical Engineering*.
- Reese, R., Charron, G., Nadjar, A., Aubert, I., Thiolat, M.-L., Hamann, M., Richter, A., Bezard, E., and Meissner, W. G. (2009). High frequency stimulation of the entopeduncular nucleus sets the cortico-basal ganglia network to a new functional state in the dystonic hamster. *Neurobiology of disease*, 35(3):399–405.
- Ruiz, M. C. M., Guimarães, R. P., and Mortari, M. R. (2022). Parkinson’s disease rodent models: Are they suitable for dbs research? *Journal of Neuroscience Methods*, 380:109687.
- Statz, M., Kober, M., Schleuter, F., Bathel, H., Plocksties, F., Timmermann, D., van Rienen, U., Fauser, M., and Storch, A. (2023a). Effects of deep brain stimulation in the subthalamic nucleus (stn-dbs) on cellular plasticity in catecholaminergic systems in a hemiparkinsonian rat model. *Brain Stimulation: Basic, Translational, and Clinical Research in Neuromodulation*, 16(1):313–314.
- Statz, M., Schleuter, F., Weber, H., Kober, M., Plocksties, F., Timmermann, D., Storch, A., and Fauser, M. (2023b). Subthalamic nucleus deep brain stimulation does not alter growth factor expression in a rat model of stable dopaminergic deficiency. *Neuroscience Letters*, 814:137459.
- Ungerstedt, U. (1968). 6-hydroxy-dopamine induced degeneration of central monoamine neurons. *European journal of pharmacology*, 5(1):107–110.
- van Dongen, M. N. and Serdijn, W. A. (2016). Does a coupling capacitor enhance the charge balance during neural stimulation? an empirical study. *Medical & biological engineering & computing*, 54:93–101.
- VARTA (2019). *Technical Handbook CoinPower - Rechargeable Li-Ion Button Cells Generation A4*. version 1.0.
- Zhang, K. K., Matin, R., Gorodetsky, C., Ibrahim, G. M., and Gouveia, F. V. (2024). Systematic review of rodent studies of deep brain stimulation for the treatment of neurological, developmental and neuropsychiatric disorders. *Translational Psychiatry*, 14(1):186.